Helicity Asymmetry E for $\gamma p \to \pi^0 p$ in the Resonance Region

Chan Kim

The George Washington University

Dissertation Defense
Nov. 23, 2021

Overview

Motivation

Baryon Spectroscopy

- Baryon Spectroscopy is the study of excited nucleon states.

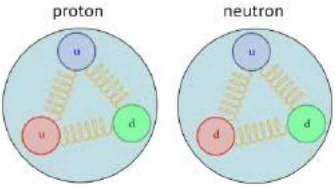

Excitation

Particle	J^P	overall	$N\gamma$	$N\pi$	$\Delta\pi$	$N\sigma$	$N\eta$	ΛK	ΣK	$N\rho$	$N\omega$	$N\eta'$
N	$1/2^+$	****										
$N(1440)$	$1/2^+$	****	****	****	****	***						
$N(1520)$	$3/2^-$	****	****	****	****	**	****					
$N(1535)$	$1/2^-$	****	****	****	***	*	****					
$N(1650)$	$1/2^-$	****	****	****	***	*	****	*				
$N(1675)$	$5/2^-$	****	****	****	****	***	*	*	*			
$N(1680)$	$5/2^+$	****	****	****	****	***	*	*	*			
$N(1700)$	$3/2^-$	***	**	***	***	*	*			*		
$N(1710)$	$1/2^+$	****	****	****	*		***	**	*	*	*	
$N(1720)$	$3/2^+$	****	****	****	***	*	*	****	*	*	*	
$N(1860)$	$5/2^+$	**	*	**		*	*					
$N(1875)$	$3/2^-$	***	**	**	*	**	*	*	*	*	*	
$N(1880)$	$1/2^+$	***	**	*	**	*	*	**	**		**	
$N(1895)$	$1/2^-$	****	****	*	*	*	****	**	**	*	*	****
$N(1900)$	$3/2^+$	****	****	**	**	*	*	**	**		*	**
$N(1990)$	$7/2^+$	**	**	**			*	*	*			
$N(2000)$	$5/2^+$	**	**	*	**	*	*				*	
$N(2040)$	$3/2^+$	*		*								
$N(2060)$	$5/2^-$	***	***	**	*	*	*	*	*	*	*	
$N(2100)$	$1/2^+$	***	**	***	**	**	*	*		*	*	**
$N(2120)$	$3/2^-$	***	***	**	**	**		**	*		*	*
$N(2190)$	$7/2^-$	****	****	****	****	**	*	**	*	*	*	
$N(2220)$	$9/2^+$	****	**	****			*	*	*			
$N(2250)$	$9/2^-$	****	**	****			*	*	*			
$N(2300)$	$1/2^+$	**		**								
$N(2570)$	$5/2^-$	**		**								
$N(2600)$	$11/2^-$	***		***								
$N(2700)$	$13/2^+$	**		**								

- Most existing data from $N\pi$
- Current $N\gamma$ data only up to 1.7 GeV
- Missing resonance problem above 1.7 GeV

Theoretical Predictions

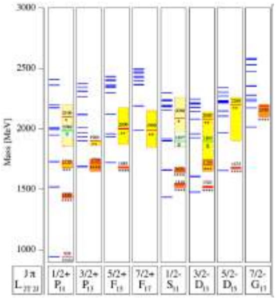

Constituent Quark Models

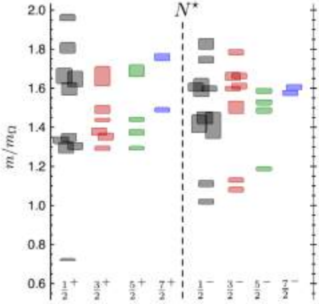

Lattice QCD

- CQMs fairly comparable to experimental results in $W \leq 1.7$ GeV
- CQMs have different effective degrees of freedom $\rightarrow$ different predictions of resonances
  - One Gluon Exchange model, Goldstone boson exchange model, quark-diquark model, instanton exchange model, *etc*.

- LQCD N^* resonance spectrum calculated using unphysical π^0 mass of 396 MeV
  - Quantitatively incomparable to experimental results or CQM results.

Photoproduction Amplitudes: Helicity

• Eight possible helicity states ($2 \times 2 \times 2$): two helicity states from each photon (λ_k), initial proton (λ_1) , and recoiling proton (λ_2).

$$\lambda_k \in \Big\{ \pm 1 \Big\}, \qquad \lambda_1 \in \Big\{ \pm \frac{1}{2} \Big\},$$
$$\lambda_q \in \Big\{ 0 \Big\}, \qquad \lambda_2 \in \Big\{ \pm \frac{1}{2} \Big\}.$$

•The total initial helicity states $\lambda_i = \lambda_k - \lambda_1$ and final helicity states $\lambda_f = \lambda_q - \lambda_2$.

$$\lambda_i \in \Big\{ \pm \frac{1}{2}, \pm \frac{3}{2} \Big\}, \qquad \lambda_f \in \Big\{ \pm \frac{1}{2} \Big\}$$

• From *T Matrix* to *Helicity Amplitudes* of $\vec{\gamma}\vec{p} \to \pi^0 p$:

$$\langle \mathbf{q}\ m_{s'} | \, T \, | \mathbf{k}\ m_s\ \lambda \rangle = \boxed{\langle m_{s'} | \, \mathbf{J} \, | m_s \rangle} \cdot \epsilon_\lambda(\mathbf{k}) \quad \Rightarrow \quad H_i(\theta) \equiv \langle \lambda_2 | \, \mathbf{J} \, | \lambda_1 \rangle$$

• 4 Complex Helicity Amplitudes:

$$H_1(\theta) = \left\langle +\frac{3}{2} \middle| \, \mathbf{J} \, \middle| +\frac{1}{2} \right\rangle \qquad H_2(\theta) = \left\langle +\frac{1}{2} \middle| \, \mathbf{J} \, \middle| +\frac{1}{2} \right\rangle$$
$$H_3(\theta) = \left\langle +\frac{3}{2} \middle| \, \mathbf{J} \, \middle| -\frac{1}{2} \right\rangle \qquad H_4(\theta) = \left\langle +\frac{1}{2} \middle| \, \mathbf{J} \, \middle| -\frac{1}{2} \right\rangle$$

Polarization Observables

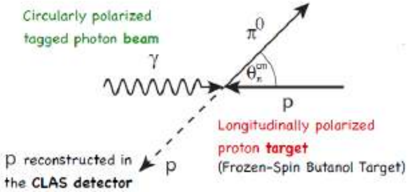

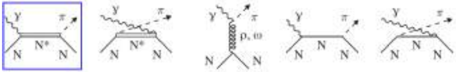

1^{st}: s-channel with the intermediate resonance state (N^* or Δ^*)
2^{nd}: u-channel with a resonance
3^{rd}: t-channel where a vector meson is exchanged
4^{th} & 5^{th}: Born terms - exchanged particle is a nucleon

- 8 helicity states $\rightarrow$ 8 complex helicity amplitudes $\rightarrow$ 16 measurable observables
  - a real part and a phase for each complex helicity amplitude
- A set of eight well-chosen observables $\longrightarrow$ four complex helicity amplitudes via PWA

Photon	Target				Recoil			Target + Recoil			
	-	-	-	-	x'	y'	z'	x'	x'	z'	z'
	-	x	y	z	-	-	-	x	z	x	z
unpolarized	σ_0		T			P		$T_{x'}$	$-L_{x'}$	$T_{z'}$	$L_{z'}$
linearly pol.	$-\Sigma$	H	$(-P)$	$-G$	$O_{x'}$	$(-T)$	$O_{z'}$	$(-L_{z'})$	$(T_{z'})$	$(-L_{x'})$	$(-T)$
circular pol.		F		$-E$	$-C_{x'}$		$-C_{z'}$				

Helicity Asymmetry E

- Double polarization observable E is the helicity asymmetry of the cross section:

$$E = \frac{\sigma_{1/2} - \sigma_{3/2}}{\sigma_{1/2} + \sigma_{3/2}} \qquad \text{for } \frac{1}{2} \;\&\; \frac{3}{2} \text{ are total helicity states}$$

- $\frac{d\sigma}{d\Omega}$ of polarized beam & polarized target for E (theo. & exp.):

$$\left(\frac{d\sigma}{d\Omega}\right)_{\frac{1}{2},\frac{3}{2}} = \frac{d\sigma_0}{d\Omega}(1 \mp (P_z P_\lambda)_{\frac{1}{2},\frac{3}{2}} E) \qquad \left(\frac{d\sigma}{d\Omega}\right)_{\frac{1}{2},\frac{3}{2}} = \frac{N_{\frac{1}{2},\frac{3}{2}}}{A \cdot F \cdot \rho \cdot \Delta x_i}$$

- E is measured via:

$$\boxed{E = \left[\frac{1}{D_f}\right] \left[\frac{1}{P_z P_\lambda}\right] \left[\frac{N_{\frac{1}{2}} - N_{\frac{3}{2}}}{N_{\frac{1}{2}} + N_{\frac{3}{2}}}\right]}$$

D_f = dilution factor

P_z = Polarization of target in $\hat{z}$

P_λ = Polarization of beam

$N_{\frac{3}{2},\frac{1}{2}}$ = # of events

Experiment

JLab Continuous e^{-} Beam Accelerator (6 Gev, before upgrade to 12 GeV)

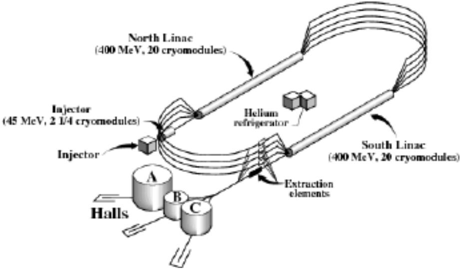

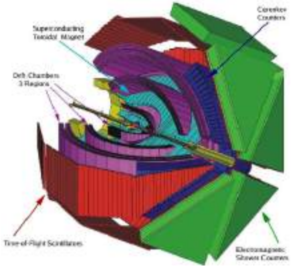

Electron Beam Energy (GeV)	Photon Beam Polarization	# of Events (M)	Observable
1.645	Circular	∼ 1000	E
2.478	Circular	∼ 2000	E
2.751	Linear	∼1000	G
3.538	Linear	∼2000	G
4.599	Linear	∼3000	G

Hall B g9a/FROST run from 12/2007 ∼ 2/2008

Circularly Polarized Photon Beam

Linearly Polarized Electron Beam $\xrightarrow{\textit{Bremsstrahlung}}$ Circularly Polarized Photon Beam

- Polarization transfer:

$$P(\gamma) = P(e)\frac{4x - x^2}{4 - 4x + 3x^2}$$

$$x = \frac{k}{E_0} = \frac{\text{photon energy}}{\text{incident electron energy}}$$

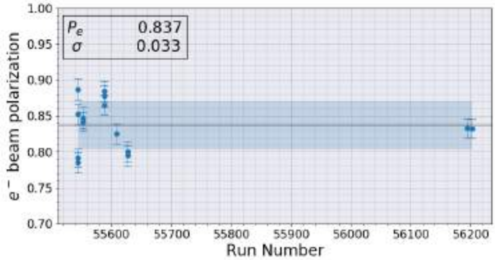

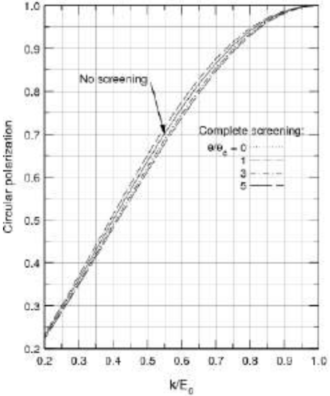

FROzen Spin Target (FROST) system

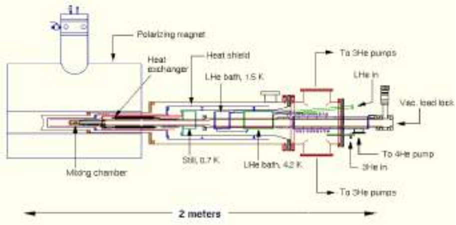

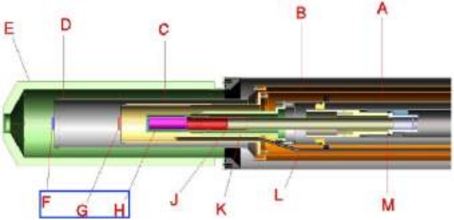

(A) Primary head exchanger, (B) 1 K heat shield, (C) Holding coil, (D) 20 K heat shield, (E) Outer vacuum cup, (F) Polyethylene target, (G) Carbon target, (H) Butanol target, (J) Target insert, (K) Mixing chamber, (L) Microwave waveguide, and (M) Kapton cold seal

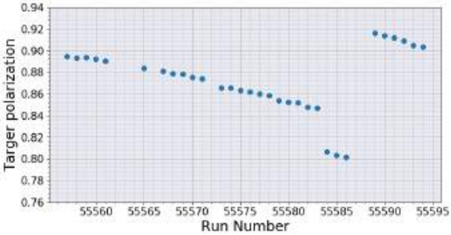

- Dynamic Nuclear Polarization technique:

$$P = \tanh\left(\frac{\vec{\mu}\cdot\vec{B}}{kT}\right)$$

- Polarization: +82% & -85%
- Temperature: 28∼30 mk
- Spin relaxation time: 1600 hrs for +Pol.
  2800 hrs for -Pol

Butanol & Carbon Targets

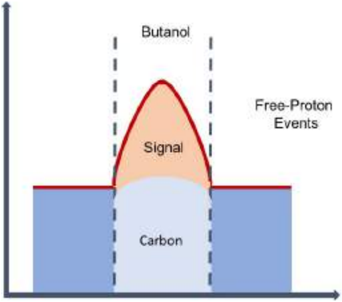

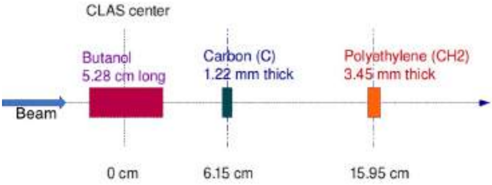

- Butanol target (C_4H_9OH) consists of polarized hydrogen (free-nucleons) & unpolarized carbon and oxygen (bound-nucleons)
- Fermi motion of bound-nucleons → broader missing mass M_{π^0} distribution
- Carbon target consists of unpolarized bound-nucleon
- Scale carbon target events & subtract from butanol target events

Event Selection

Butanol z-vertex selection range

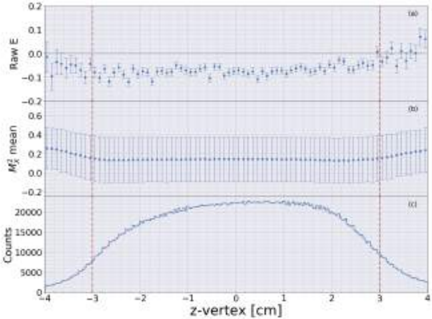

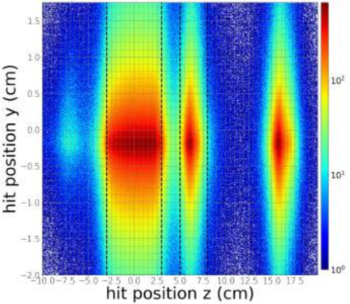

- Butanol selection range $z = [-3,\ 3]$ cm
- Butanol target thickness 5.28 cm
- Raw helicity asymmetry E starts to diverge from the expected value at $z = -3, 3$ cm
  - $E_\gamma \in [0.84,\ 1.27]$ GeV
  - $\cos\theta_{cm} \in [-0.97,\ 0.0]$
  - E expected to be negative by PWA pred.
  - absence of free nucleon outside $z = -3, 3$ cm
- M_X^2 mean starts to shift from $M^2_{\pi^0}$ at $z = -3, 3$ cm

Carbon z-vertex selection range

- Carbon selection range $z = [5,\ 8]$ cm
- Carbon target thickness 0.12 cm

- Poor tracking in forward angles
  - $\longrightarrow$ dispersed carbon events in $z = [5,\ 8]$ cm
- Hydrogen contamination
  - $\longrightarrow$ sharp peak in M_X^2 distribution
  - $\longrightarrow$ potential ice formation in $z = [6,\ 7.5]$ cm
- Could have tighter selection range
  - $\longrightarrow$ poor fitting results

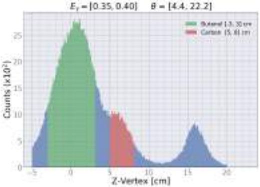

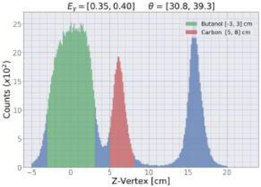

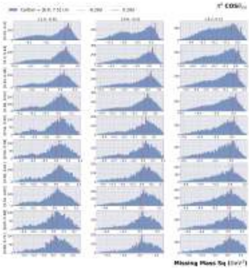

$z = [5.0,\ 7.5]$ cm

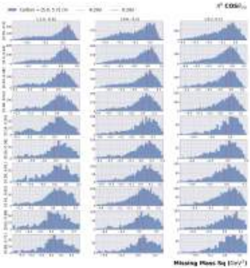

$z = [5.0,\ 6.0]$ cm

Binning

- Separate binning for $E_e = 1.6$ GeV & $E_e = 2.4$ GeV data sets
  - -different π^0 concentrations
- Subset of events (red vertical lines) used for determining bins
  - -to ensure evenly spaced π^0 events throughout bins
- Each bin contains approx. the same number of events.

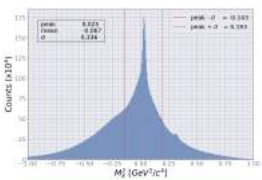

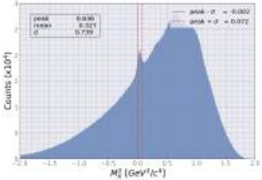

- $E_e = 1.6$ GeV data
  - -Higher π^0 vs background ratio

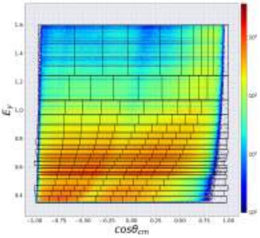

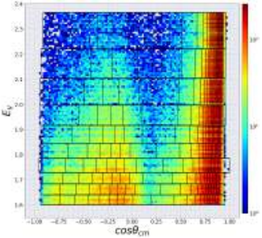

- $E_e = 2.4$ GeV data
  - -Lower π^0 vs background ratio
  - -π^0 only 5% of total
  - -Tighter selection range

M_X^2 Selection: $M_X^2 = (E_\gamma + m_{p_1} - E_{p_2})^2 - (\vec{p}_\gamma - \vec{p}_{p_2})^2$

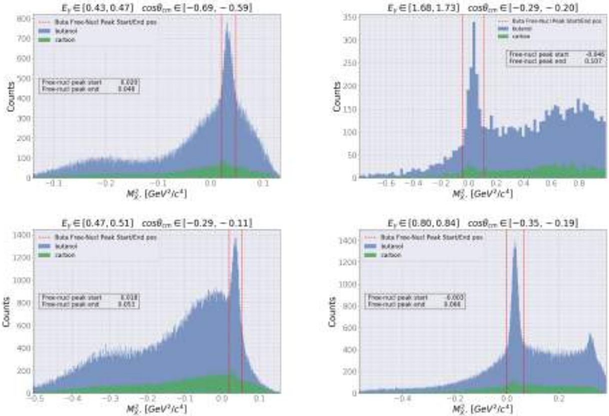

- Select a subset of events w/ the highest ratio of free nucleon events / bound nucleon events.
- Only this subset of events is used for the final computation of E.
- Different free nucleon selection range for each bin.
  - –determined during scale factor calculations

Other Event Selection steps

- Inactive CLAS regions
- Energy Loss and Momentum Corrections
- Low Momentum Selection
- Inefficient Time-of-Flight paddles
- Particle ID: Proton selection
- Photon identification
- Transverse event vertex selection

Application of Machine Learning

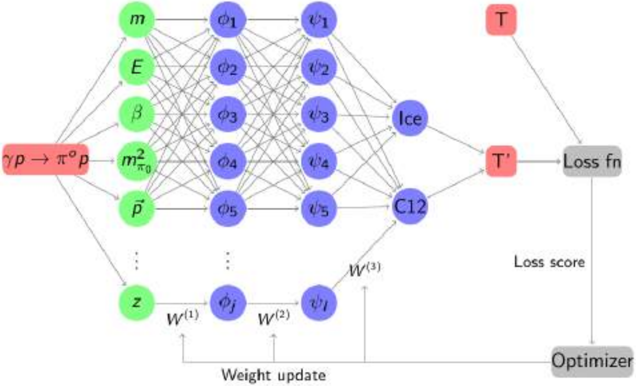

Target classification

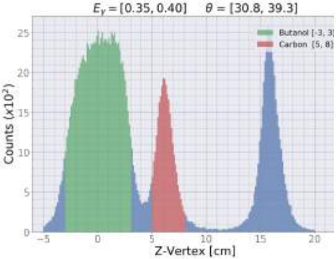

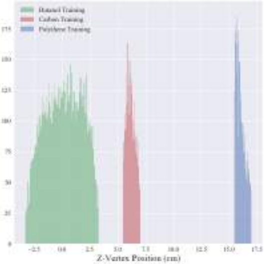

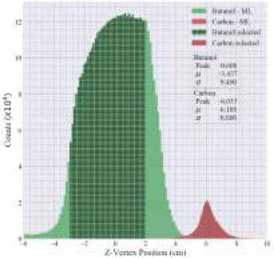

- Randomly select events with z-vertex positions in close proximity of known target location
- Ratio of butanol/carbon training data = Ratio of butanol/carbon testing data
  - Butanol $\in$ [-3.3, 3.3]cm
  - Carbon $\in$ [5.5, 7.0]cm
  - Polythene $\in$ [15.5, 17.0]cm

- Classified carbon events from butanol in z-vertex $\in$ [2.5, 4.5]cm
- Some carbon events in polythene regions & Polythene events in the butanol region.

Hydrogen Contamination

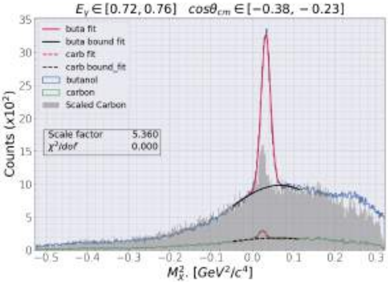

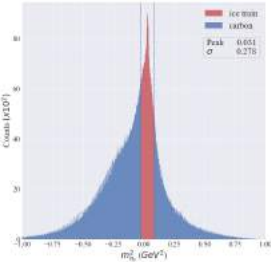

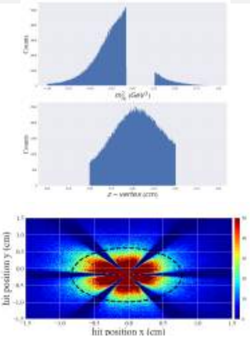

- Tight selection on carbon $M^2_{\pi_0}$ as ice
  - –Bound-nucleon (fermi p) $\rightarrow$ broader m^2 distribution
  - –Sharper peaks from free-nucleon (ice) & Broad background from bound-nucleon (carbon)

- Randomly select carbon train data within:
  - –Classified as carbon events in previous target classification distribution
  - –Missing mass squared $\notin [-\sigma, \sigma]$
  - –Z-vertex position $\notin [6.5, 7.5]$

Final Result of ML: ICE vs CARBON

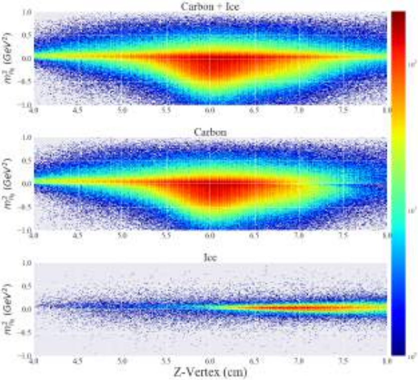

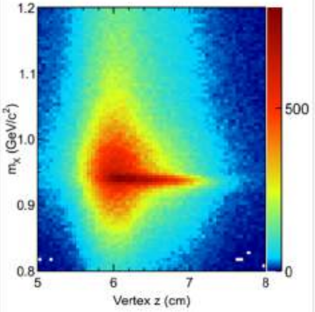

Figure 3: Missing-mass distribution as a function of the MVRT z vertex of the π+. The shape of the missing-mass distribution strongly changes with z. Event selection: $p_{\pi} > 0.2$ GeV/c and $\theta_{\pi} > 20^{\circ}$.

[Result from USC for $\gamma p \rightarrow \pi^+ n$]

- Classified ice events from Carbon target in z-vertex $\in$ [6.0, 7.5]cm
- It is likely that ice was formed in the 20 K heat shield in between carbon and polythene targets.

Helicity Asymmetry E

Initial Scale Factor

- Bound nucleons $\rightarrow$ Fermi momentum $\rightarrow$ broader side-bands of M_X^2 distribution than free-nucleon events.

$$E_{p1,\text{bound}} = \sqrt{m_p^2 + p_{\text{Fermi}}^2},$$

$$M_{\pi^0}^2 = (E_\gamma + m_{p1} - E_{p2})^2 - (\vec{p}_\gamma + \vec{p}_{\text{Fermi}} - \vec{p}_2)^2.$$

- $[\mu - 2.0\sigma,\ \mu - 1.5\sigma]$ for $E_e = 1.6$ GeV
- $[\text{peak} + 1.0\sigma,\ \text{peak} + 1.5\sigma]$ for $E_e = 2.4$ GeV

- χ^2 minimized to obtain initial scale factor:

$$\chi^2 = \sum_i \frac{(N_i^B - \alpha N_i^C)^2}{N_i^B + \alpha^2 N_i^C},$$

$$N_i^B = \int_{\mu-2\sigma}^{\mu-1.5\sigma} n_b \ dm_x^2,$$

$$N_i^C = \int_{\mu-2\sigma}^{\mu-1.5\sigma} n_c \ dm_x^2,$$

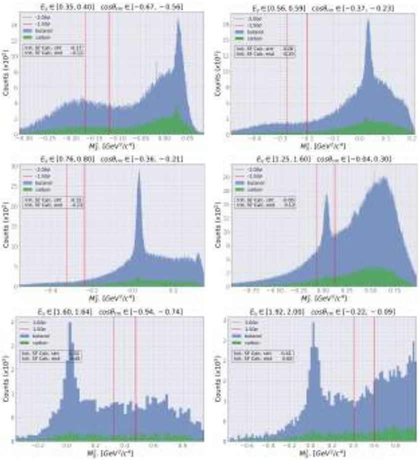

First free proton peak extraction

- Using initial scale factors, butanol M_X^2 distrib. are subtracted by scaled carbon M_X^2 distrib.
- The residuals are fitted with a Gaussian.
- *peak* $\pm\, 3\sigma$ of fitted Gaussian is set as start/end positions of free nucleon peaks

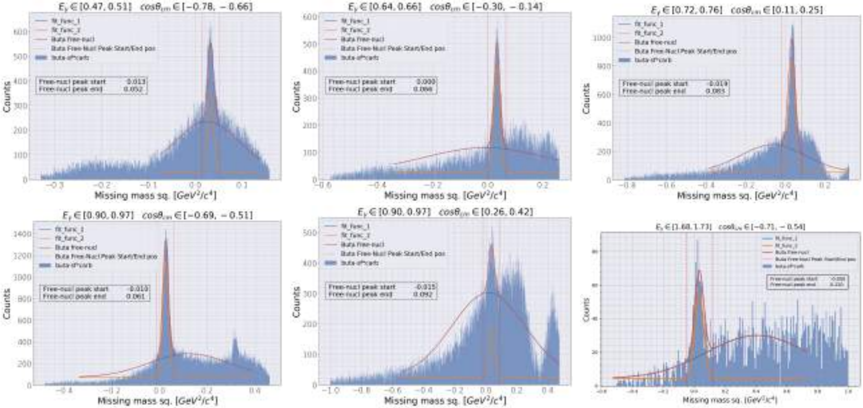

Discarded Bins

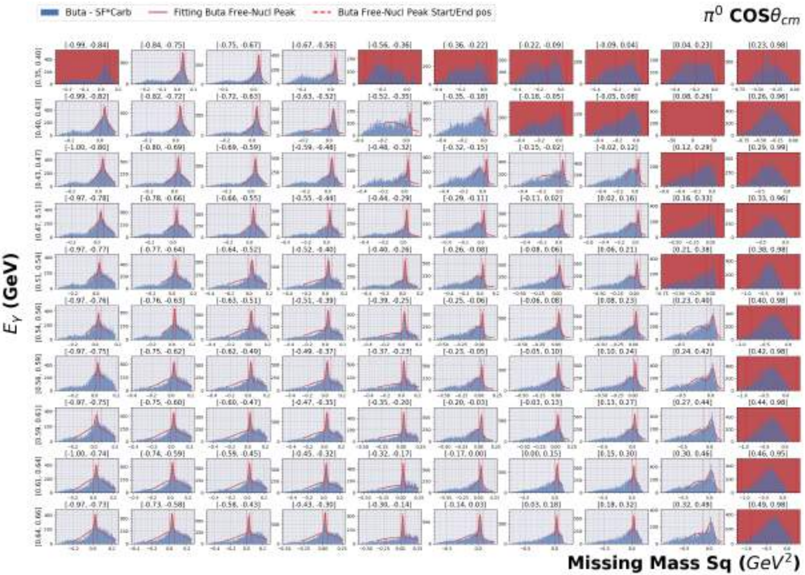

Final Scale Factor

- Using extracted free nucleon peak ranges, fitting ranges are determined.

- Both butanol and carbon free nucleon peaks fitted with a Gaussian

$$f(m_X^2) = A_1 \cdot exp\left(-\frac{(m_x^2 - \mu_{pk})^2}{2\sigma_{pk}^2}\right) + f_{bnd}(m_x^2).$$

- Gaussian or 4th order polyn. to fit background:

- χ^2 minimized to obtain the scale factor:

$$\chi^2 = \sum_i^N \frac{[B_{bnd}(i) - \alpha \ C_{bnd}(i)]^2}{B_{bnd}(i) - \alpha^2 \ C_{bnd}(i)}$$

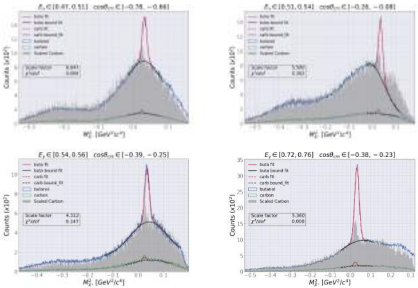

(1) Scaled carbon M_X^2 distribution correctly represent butanol background events.
(2) Angular dependence, causing discrepancies in M_X^2 distributions for butanol and carbon targets.
(3,4) strong hydrogen contamination on carbon target where scaled carbon fails to correspond to butanol background events.

Second free proton peak extraction

- Using improved scale factors, butanol M_X^2 distrib. are subtracted by scaled carbon M_X^2 distrib.
- The residuals are fitted with a Gaussian.
- *peak* $\pm 3\sigma$ of fitted Gaussian are set as start/end positions of free nucleon peaks
- Extracted free nucleon ranges are used in the final M_X^2 selection in event selection process.

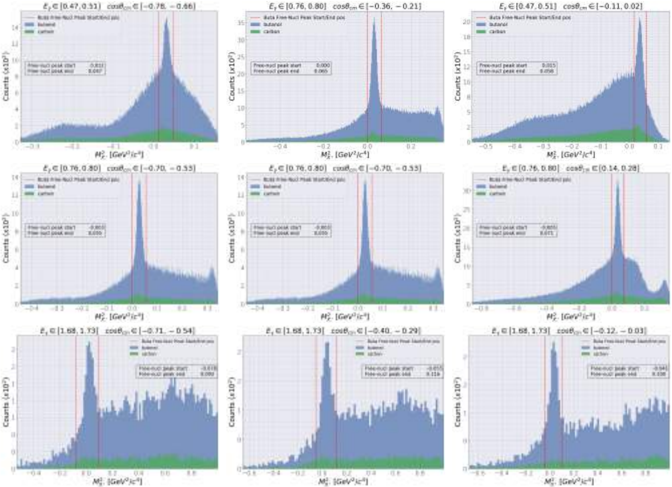

Dilution Factor D_f

- D_f computed in the final free nucleon peak extraction regions.
- B_{bnd} obtained by integrating the fitting fn. that describes background of butanol M_X^2 distrib.
- B_{tot} obtained by multiplying the # of counts in each bin by the width of the bin.
- $D_f\big|_{\text{low lim}} = \frac{\text{free H in butanol}}{\text{total nucleon in butanol}} = \frac{10}{74} \cong 0.135$

$$D_f = \frac{B_{tot} - B_{bnd}}{B_{tot}},$$

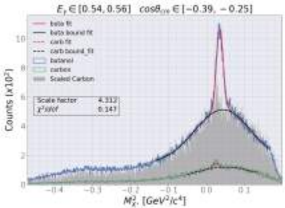

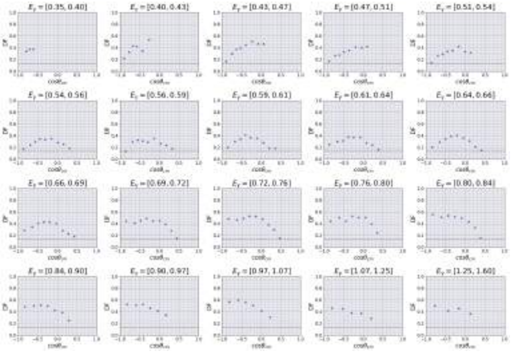

Extraction of Helicity Asymmetry E

- Compute E from the events that lie within the extracted free nucleon peak regions:

$$\boxed{E = \left[\frac{1}{D_f}\right]\left[\frac{1}{P_z P_\lambda}\right]\left[\frac{N_{\frac{1}{2}} - N_{\frac{3}{2}}}{N_{\frac{1}{2}} + N_{\frac{3}{2}}}\right]}$$

$D_f =$ dilution factor
$P_z =$ Polarization of target in $\hat{z}$
$P_\lambda =$ Polarization of beam
$N_{\frac{3}{2},\frac{1}{2}} = \#$ of events

- Statistical uncertainty sources: counting stats, target polarization, beam polarization, fitting routines used in scale factor and dilution factors.

$$\sigma_E^2 = \sigma_{N_{1/2}}^2\left(\frac{\partial E}{\partial N_{1/2}}\right)^2 + \sigma_{N_{3/2}}^2\left(\frac{\partial E}{\partial N_{3/2}}\right)^2 + \sigma_{P_T}^2\left(\frac{\partial E}{\partial P_T}\right)^2 + \sigma_{P_\gamma}^2\left(\frac{\partial E}{\partial P_\gamma}\right)^2 + \sigma_{D_f}^2\left(\frac{\partial E}{\partial D_f}\right)^2$$
$$= E^2\left[\left(\frac{\sigma_{D_f}}{D_f}\right)^2 + \left(\frac{\sigma_{P_\gamma}}{P_\gamma}\right)^2 + \left(\frac{\sigma_{P_T}}{P_T}\right)^2 + \frac{4N_{1/2}N_{3/2}}{N_{tot}(N_{3/2} - N_{1/2})^2}\right],$$

Results

$E_\gamma = [0.35, 1.6]$ GeV

- CBELSA experimental result - $\gamma p \to \pi^0 p \to \gamma\gamma p$
- CBELSA data has more statistics in forward angles $\cos\theta_{cm} = [0.5, 1.0]$.
- FROST data has more statistics in $\cos\theta_{cm} = [-0.97, 0.25]$.
- PWA predictions from SAID, BnGa, and MAID.

- $\Delta(1232)$ becomes insignificant and more non-resonant terms contribute (u- and t-channel) at $E_\gamma \approx 0.5$ GeV.
- Oscillatory behaviors indicate the emergence of more resonances
- MAID only valid under $E_\gamma \leq 1.6$ GeV.

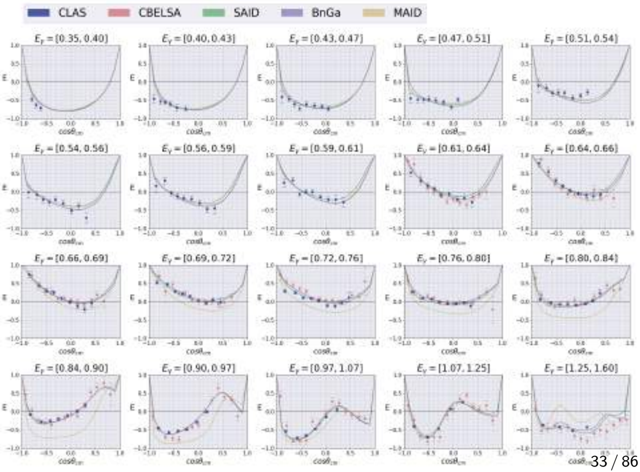

$E_\gamma = [1.6, 2.4]$ GeV

- In $E_\gamma = [0.35, 1.92]$ GeV, SAID and BnGa show agreements with our results.
- In $E_\gamma = [1.92, 2.10]$ GeV, SAID starts to deviate.
- SAID is less model dependent than BnGa and more data-driven.
- Addition of our result into the SAID database will reduce PWA models' discrepancies.

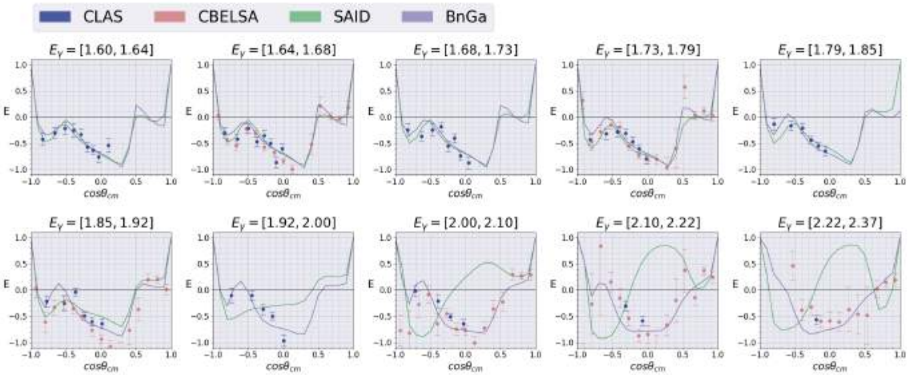

New SAID solution - KI21

- Our result added to SAID database $\longrightarrow$ new SAID prediction (KI21)
- Previous SAID solution (MA19) included CBELSA results.
- Slight changes in SAID prediction starting at $E_\gamma = 0.84$ GeV.

- Significant improvements starting at $E_\gamma \geq 1.79$ GeV.
- Fewer data points, but with lower stat. uncertainties than CBELSA
  - More impacts on SAID predictions.
  - Larger angular bin size to reduce stat. uncertainty.

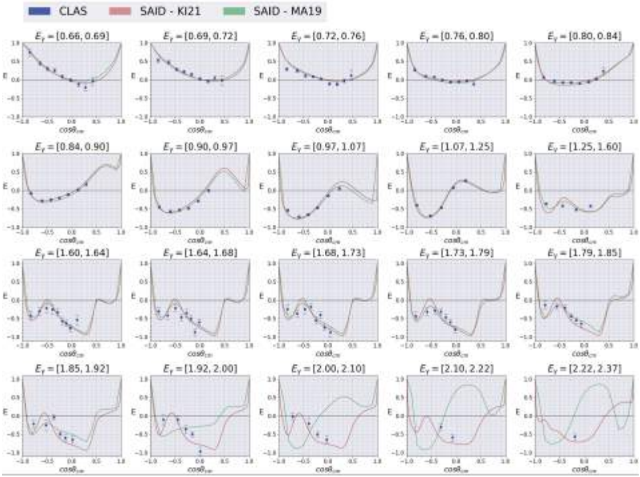

Future Works

- Systematic studies $\rightarrow$ Analysis Note to CLAS HSWG &
  CLAS Collab. paper for Phys. Rev. C
- Momentum correction software rewrite for outgoing protons
  - Possible cause for θ dependence of M_X^2 distributions.
  - ELOSS assumes γ beams aligned with z-axis and no ϕ dependence.
  - Momentum correction corrects ϕ dependence.
- Machine learning improvements
  - Extract training data separately in each angle and energy bin.
  - Regularization methods to avoid overfitting.
  - Bayesian Neural Network to quantify uncertainties in training data.

Thank you

BACK UP

Motivation BACK UP

γp channel - resonances overlap

All γp channels

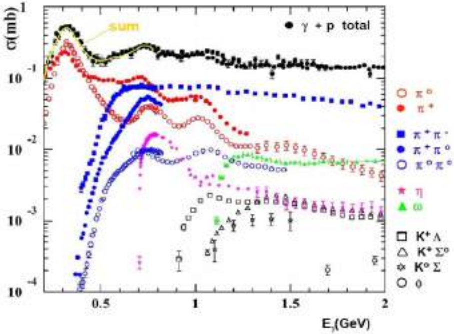

$\gamma p \to \pi^0 p$ resonances

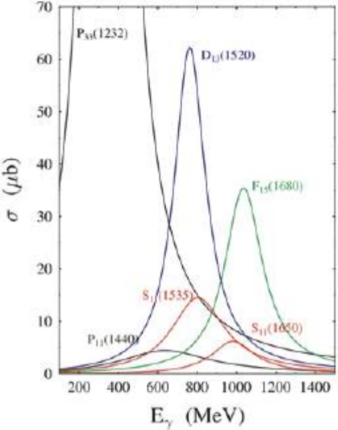

- Most resonances' widths larger than spacing distances between each resonance
- Second and third resonance region $E_\gamma \approx [0.5,\ 2.4]$ GeV
- Decay via strong interaction: $\tau \approx 10^{-24}$ sec & $\Gamma \approx 0.1 \sim 0.3$ GeV.

Constituent Quark Models (CQMs)

- Constituent quarks = valence quarks + gluons + sea quarks
- Many different CQMs postulate various forms of short-range interactions
  - One Gluon Exchange model, Goldstone boson exchange model, quark-diquark model, instanton exchange model, *etc*.
- Fairly comparable to experimental results in $W \leq 1.7$ GeV

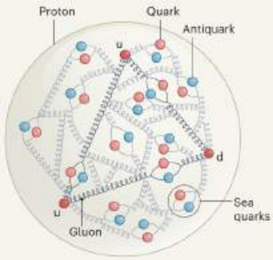

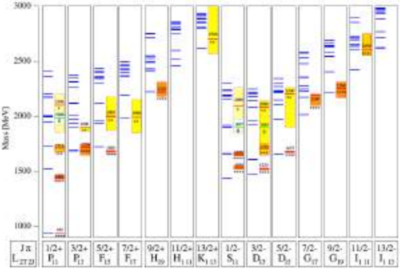

- Different CQMs have different effective degrees of freedom (dof), causing different predictions of resonance states & parameters of resonances (mass, width, etc).
  - Fewer effective dof predicts lesser number of resonances.
  - Quark-diquark model predicts less, but still larger than experimentally found resonances
  - Experimental results to help configure correct effective dof

Lattice QCD

- Space-time continuum replaced by space-time lattice:
  - valence quarks, sea quarks, and gluons propagate along grids.
  - Quark fields q_n at every lattice site and gluon fields $U_{n\mu}$ at every lattice link.
- Physical quantities computed by path integrals using Monte Carlo simulation in the lattice.
- Quark masses used in LQCD bigger than actual quark masses.
  - Extrapolate to approximate to real values.
- N^* and Δ^* resonance spectrum calculated using unphysical π^0 mass of 396 MeV
  - Quantitatively incomparable to experimental results or CQM results, but qualitatively in some agreement.

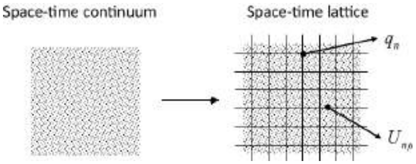

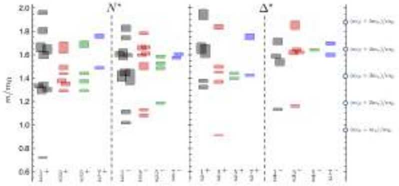

Pion photoproduction cont.

	Composition	I^G	I_3	J^{PC}	Mass (MeV)	Lifetime (s)	$c\tau$ (m)	Decay Modes	BR(%)
π^+	$u\bar{d}$	1^-	1	0^-	139.57	2.6×10^{-8}	7.80	$\mu^+ + \nu_\mu$	99.9
								$e^+ + \nu_e$	1.24×10^{-4}
								$\pi^0 + e^+ + \nu_e$	1.00×10^{-8}
π^-	$d\bar{u}$	1^-	-1	0^-	139.57	2.6×10^{-8}	7.80	$\mu^- + \bar{\nu_\mu}$	99.9
								$e^- + \bar{\nu_e}$	1.24×10^{-4}
								$\pi^0 + e^- + \bar{\nu_e}$	1.00×10^{-8}
π^0	$u\bar{u}$ or $d\bar{d}$	1^-	0	0^{-+}	134.97	8.4×10^{-17}	25.1×10^{-9}	2γ	98.8
								$\gamma + e^- + e^+$	1.17×10^{-2}
								$2e^- + 2e^+$	3.34×10^{-5}
								$e^- + e^+$	6.46×10^{-8}

- Long lifetime of charged pions (2.6×10^-8 s) $\rightarrow$ decay via weak interactions ($10^{-8} \sim 10^{-15}$ s)
- π^0 short lifetime of 8.4×10^{-17} s $\rightarrow$ electromagnetic decay
- No direct detections of π^0 in pion photoproduction experiments
- Two methods of reconstructing π^0
  - Measure 2γ and reconstruct π^0 - CBELSA approach
  - Use kinematics of incident γ, initial proton and recoiling proton to reconstruct π^0 - Our approach

Photoproduction Amplitudes: CGLN

- Chew-Goldberger-Low-Nambu (CGLN) amplitudes:

$$\frac{d\sigma}{d\Omega} = \frac{q}{k} |\langle f | \mathcal{F}_\lambda | i \rangle|^2, \tag{1}$$

- $\mathcal{F}_\lambda$ decomposed in to current operator $\mathbf{J}$ and photon pol. vector $\boldsymbol{\epsilon}_{\lambda_\gamma}$

$$\langle m_{s'} | \mathcal{F}_\lambda | m_s \rangle = \langle m_{s'} | \mathbf{J} | m_s \rangle \cdot \boldsymbol{\epsilon}_\lambda(\mathbf{k}), \tag{2}$$

- In terms of Pauli-spin matrices $\boldsymbol{\sigma}$ and four CGLN amplitudes $\mathcal{F}_1, \ldots, \mathcal{F}_4$

$$\begin{aligned} \mathbf{J} &= i\mathcal{F}_1 \boldsymbol{\sigma} + \mathcal{F}_2 \frac{(\boldsymbol{\sigma} \cdot \boldsymbol{q})(\boldsymbol{\sigma} \times \boldsymbol{k})}{qk} + i\mathcal{F}_3 \frac{\boldsymbol{\sigma} \cdot \boldsymbol{k}}{qk} \boldsymbol{q} + \mathcal{F}_4 \frac{\boldsymbol{\sigma} \cdot \boldsymbol{q}}{q^2} \boldsymbol{q}, \\ \mathcal{F}_\lambda &= \boldsymbol{J} \cdot \boldsymbol{\epsilon}_\lambda \\ &= i\mathcal{F}_1 \boldsymbol{\sigma} \cdot \hat{\epsilon_{\boldsymbol{\lambda}}} + \mathcal{F}_2 (\boldsymbol{\sigma} \cdot \hat{\boldsymbol{q}}) \boldsymbol{\sigma} \cdot (\hat{\boldsymbol{k}} \times \hat{\epsilon_\lambda}) + i\mathcal{F}_3 (\boldsymbol{\sigma} \cdot \hat{\boldsymbol{k}})(\hat{\boldsymbol{q}} \cdot \hat{\epsilon_\lambda}) + i\mathcal{F}_4 (\boldsymbol{\sigma} \cdot \hat{\boldsymbol{q}})(\hat{\boldsymbol{q}} \cdot \hat{\epsilon_\lambda}). \end{aligned} \tag{3}$$

Photoproduction Amplitudes: Multipoles

- CGLN amplitudes expressible in terms of two multipole amplitudes - magnetic ($M_{l\pm}$) and electric ($E_{l\pm}$) amplitudes
  - l is the orbital angular momentum of the final state

- $M_{l\pm}$ and $E_{l\pm}$ as transition amplitudes caused by magnetic and electric multipole radiation.
  - For ex, E_{0+} is the transition amplitude initiated by electric dipole radiation which involves the final πN state to be in s-wave ($l = 0$).
  - M_{l-} and M_{l+} refers to transitions to the final πN state to be in p-wave ($l = 1$) with the total angular momentum of $J = 1/2$ or $J = 3/2$

- Multipole amplitudes classified - L and J of γ and πN:

Multipole	L	J	L_γ	Parity
E_{0+}	0	1/2	1	-
M_{1-}	1	1/2	1	$+$
M_{1+}	1	3/2	1	$+$
E_{1+}	1	3/2	2	$+$
E_{2-}	2	3/2	2	$+$

- CGLN amplitdues in terms of multipole amplitudes

$$\mathcal{F}_1 = \sum_{l=0}^{\infty} \left[lM_l^+ + E_l^+\right] P'_{l+1}(x) + \left[(l+1)M_l^- + E_l^-\right] P'_{l-1}(x), \ldots$$

- Multiole amplitudes in terms of CGLN amplitudes:

$$M_{l\pm} = \frac{1}{2}\begin{pmatrix}\frac{1}{l+1}\\ -\frac{1}{l}\end{pmatrix} \int_{-1}^{+1} dx \left[\mathcal{F}_1 P_l(x) - \mathcal{F}_2 P_{l\pm}(x) - \mathcal{F}_3 \frac{P_{l-1}(x) - P_{l+1}(x)}{2l+1}\right], \ldots$$

Partial Wave Analysis

- For single resonance: S-matrix element $s_l(k)$ to the phase shift δ_l by:

$$s_l(k) = e^{2i\delta_l} = \frac{1 + i\tan(\delta_l)}{1 - i\tan(\delta_l)} = \frac{E - E_0 - i\Gamma/2}{E - E_0 + i\Gamma/2}$$

- A resonance (spike in σ) corresponds to a pole position in a complex plane:

$$E = E_0 - \frac{i\Gamma}{2}.$$

- For multiple resonances contribute to a single cross section: K-matrix formalism:

$$S = \mathbb{1} + iT = \frac{\mathbb{1} + iK}{\mathbb{1} - iK} \tag{4}$$

•′ The resonances correspond to a sum of pole positions in the K-matrix which causes K-matrix elements to vary abruptly at these poles, leading to significant phase shifts:

$$K_{ij} = \sum_{\alpha}^{n} \frac{g_{\alpha i}(m) g_{\alpha j}(m)}{m_\alpha^2 - m^2} + f_{ij}, \tag{5}$$

- $f_i j$ = non-resonant term , m_α = mass of resonances, $g_{\alpha i}$ resonance coupling to the initial state i.

$$g_{\alpha i}^2(m) = m_\alpha \Gamma_{\alpha i}(m) \tag{6}$$

$$\Gamma_\alpha(m) = \sum_i \Gamma_{\alpha i}(m) \tag{7}$$

PWA models

- Each PWA model differ in parametrizing the resonance and non-resonant terms and fitting the exp. data.

⋮

- SAID
- MAID
- BnGa
- Dynamical model

⋮

Pion Photoproduction

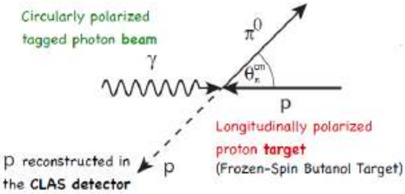

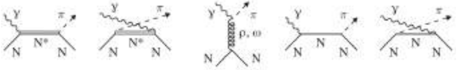

- Feynman diagrams showing contributions to π photoproduction.
  - First - s-channel with the intermediate resonance state (N^* or Δ^*)
  - Second - *u*-channel with a resonance
  - Third - *t*-channel where a vector meson is exchanged
  - 4th and 5th - Born terms where the exchanged particle is a nucleon
- Some CQMs predict some missing resonances couple strongly to γN, but weakly to πN
- Photon beam polarizable $\rightarrow$ obtain asymmetries of observables!
- Real photon beam (photoproduction $Q^2 = 0$) or quasi-real photons (electroproduction $Q^{>}0$)
- Baryon beams (protons, deuterons, & α particles) not used for resonance studies:
  - Require higher energy to excite due to higher mass
  - Final state interactions - three or more hadrons in final states
- Meson beams - long lived mesons (π^+, π^-, K^+ and K^-)
  - *isospin* $\neq 1 \rightarrow$ more isospin dof for resonances
  - large branching ratio into other meson reaction channels
  - zero spin $\rightarrow$ no polarization observables

Polarization Observables

- All photoproduction amplitudes are expressible in terms of the other! (CGLN, Multipoles, helicity, . . .)
- 8 helicity states → 8 complex helicity amplitudes → 16 measurable observables
  - a real part and a phase for each complex helicity amplitude
- a set of eight carefully chosen variables suffice to construct four complex helicity amplitudes,

- which in turn can construct CGLN amplitudes and multipole amplitudes.

- Unpolarized - $\frac{d\sigma}{d\Omega}$
- Single polar. (beam or target) - Σ, T, and P
- Double polar. (Beam add Target) - G, H, E, and F
- Double polar. (Beam and Recoil) - O_x, O_z, C_x, and C_z
- Double polar. (Target and Recoil) - T_x, T_z, L_x, and L_z

Photon	Target				Recoil			Target + Recoil			
	-	-	-	-	x'	y'	z'	x'	x'	z'	z'
	-	x	y	z	-	-	-	x	z	x	z
unpolarized	σ_0		T			P		$T_{x'}$	$-L_{x'}$	$T_{z'}$	$L_{z'}$
linearly pol.	$-\Sigma$	H	$(-P)$	$-G$	$O_{x'}$	$(-T)$	$O_{z'}$	$(-L_{z'})$	$(T_{z'})$	$(-L_{x'})$	$(-T)$
circular pol.		F		$-E$	$-C_{x'}$		$-C_{z'}$				

Current challenges in Baryon Spectroscopy

- Missing resonance problem - CQM predicts more than experimentally found
  - Wrong effective degrees of freedom in CQMs, especially at $W \geq 1.7$ GeV.
  - More experimental data in $W \geq 1.7$ GeV region can help with determining correct dof.
  - Some CQMs argue - missing resonances couple weakly to πN elastic scatterings (most of accumulated data), but strongly to γN
- Uncertainties in partial decay widths of resonances
  - Some channels simply lack experimental data: ηN, $K\Sigma$, and ωN
  - Discrepancies between PWA models

TABLE XIII. Breit-Wigner masses W_R and widths Γ (in MeV) of N and Δ resonances.

Resonance	Our estimate	Our rating	KH	CM	Kent	GWU	BnGa
$N_{3/2}$(1700)	1725±50; 190±110	***	1731±15; 110±30	1675±25; 90±40	1737±44; 250±230		1730±40; 310±60
$N_{1/2}$(1710)	1713±12; 220±180	***	1723±9; 120±15	1700±50; 90±30	1717±28; 480±330		1725±25; 200±35
$N_{3/2}$(1720)	1730±30; 320±210	****	1710±20; 190±30	1700±50; 125±70	1717±31; 380±180	1750±5; 256±22	1770±100; 650±120
$N_{3/2}$(1860)	1850±40; 260±170	**		1880±100; 180±60	1804±55; 450±185		1870±25; 150±40
$N_{3/2}$(1870)	1880±40; 270±180	—	1882±10; 95±20		1903±87; 490±310	1818; 118	1910±50; 360±80
$N_{1/2}$(1880)	1890±50; 210±100	*			1885±30; 113±44		1900±30; 300±40
$N_{3/2}$(1900)	1940±50; 340±150	*			1879±17; 498±78		1960±30; 185±40
$N_{1/2}$(1905)	1905±50; 250±150	*	1880±20; 95±30		1928±59; 414±157		
$N_{7/2}$(1990)	2020±60; 410±110	**	2005±150; 350±100	1970±50; 350±120	2086±28; 535±120		
$N_{3/2}$(2080)	2100±55; 310±110	—	2080±20; 265±40	2060±80; 300±100			2160±35; 370±50
$N_{1/2}$(2090)				2180±80; 350±100			
$N_{1/2}$(2100)	2090±100; 230±200	*	2050±20; 200±30	2125±75; 260±100			
$N_{5/2}$(2200)	2160±85; 350±50	**	2228±30; 310±50	2180±80; 400±100			2065±25; 340±40
$N_{7/2}$(2190)	2150±30; 440±110	****	2140±12; 390±30	2200±70; 500±150	2127±9; 550±50	2152±2; 484±13	2140±40; 270±50
$N_{9/2}$(2220)	2260±60; 490±115	****	2205±10; 365±30	2230±80; 500±150		2316±3; 633±17	2300±100; 450±150
$N_{9/2}$(2250)	2255±50; 420±150	****	2268±15; 300±40	2250±80; 400±120		2302±6; 628±28	2200±100; 350±100
$N_{11/2}$(2600)	2630±120; 650±250	**	2577±50; 400±100				2700±100; 900±100
$N_{13/2}$(2700)	2800±160; 600±300	**	2612±45; 350±50				3000±100; 900±150

[Klempt et al. 2010]

Experiment BACK UP

Hall B Photon Tagger

- Bremsstrahlung radiation due to slowing of electrons by EM field of radiator
  - Diamond radiator for linearly polarized photon beams
  - Gold foil radiator for circularly polarized photon beams
- Determine incoming photon energy of $\vec{\gamma}\vec{p} \rightarrow \pi^0 p$ by $E_\gamma = E_0 - E_e$
- g9a/FROST - circularly polarized photons with $E_\gamma \approx 0.4 \sim 2.4\ GeV$

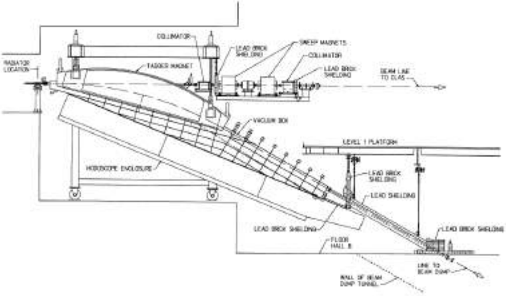

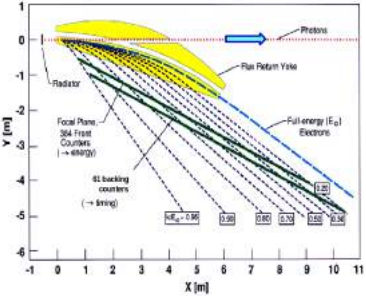

Event Selection Back up

Data Banks

- The physical quantities derived from raw signals and associated data bank names.

Quantity	Bank	Min/Max	Description
E_γ (GeV)	*TAGR*	$[0, 12]$	Closest photon energy
PID	*GPID*	$[0, 100]$	Particle ID (GEANT)
E (GeV)	*GPID*	$[0, 16]$	Energy of outgoing particle
p_x (GeV/c)	*GPID*	$[-16, 16]$	Momentum in x (lab frame)
p_y (GeV/c)	*GPID*	$[-16, 16]$	Momentum in y (lab frame)
p_z (GeV/c)	*GPID*	$[-16, 16]$	Momentum in z (lab frame)
β_c	*GPID*	$[-1, 1]$	$\frac{\lvert\vec{p}\rvert}{E}$
β_m	*GPID*	$[-1, 1]$	Beta from Time-of-Flight detector
mass (GeV)	*GPID*	$[0, 1000]$	Mass from Time-of-Flight detector
sc_time (ns)	*GPID*	$[-1000, 1000]$	Arrival time at Time-of-Flight detector
sc_len (cm)	*GPID*	$[-1000, 1000]$	Distance between event vertex to TOF counter
ntrk	*MVRT*	$[-100, 100]$	Number of tracks used to make event vertex
x-vertex (cm)	*MVRT*	$[-1000, 1000]$	X position of event vertex
y-vertex (cm)	*MVRT*	$[-1000, 1000]$	Y position of event vertex
z-vertex (cm)	*MVRT*	$[-1000, 1000]$	Z position of event vertex
ScPdHt	*SCPB*	$[0, 100000]$	10000*sector + 100*SC_PD_ID + HitID in SCR
TRIGBITS	*HEAD*	$[0, 9999999]$	Trigger Latch Word (16 bits)
NRUN	*HEAD*	$[0, 100000]$	Run Number
DCstat	*EVNT*	$[0, 50]$	Pointer to DCPB banks (=0 if drift chamber not involved)
SCstat	*EVNT*	$[0, 50]$	Pointer to SCPB banks (=0 if TOF not involved)

Initial Reaction Channel Filter

- Initial selection for $\gamma p \to \pi^0 p$ reaction channel among all possible reaction channels:

1. Select events with photon candidates that contain readings from both E- and T- counters of the tagger system.
2. Select events with one positively charged outgoing particles: e^+, π^+, K^+ and protons
3. Filter out events from miscalibration and malfunctioning parts of Time of Flight system and Drift chambers.
4. Compute basic kinematics: momentum, energy, angle, *etc*.

Energy Loss & Momentum Corrections

- The ELOSS computes energy loss of the outgoing particles while traveling inside:
  - The butanol target, target cell wall, mixing chamber, holding coils, start counters, and DC air gap
- The z-vertex dependence of M_X^2 distrib. inside the butanol target region have been remedied.

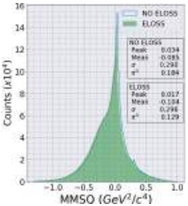

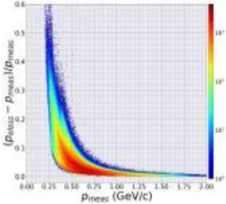

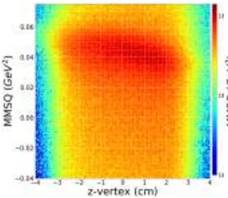

M_X^2 BEFORE

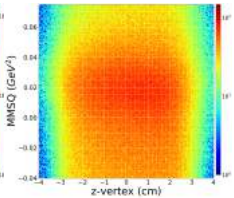

M_X^2 AFTER

- ϕ dependence remedied.
- Difference of measured momentum from the DC (p_{dc}) and calculated momentum ($p(\theta_{lab})$)

  -$\Delta p = p(\theta_{lab}) - p_{dc}$

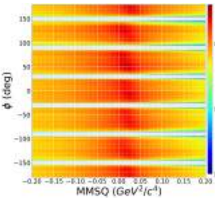

ϕ BEFORE

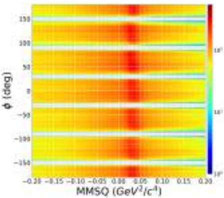

ϕ AFTER

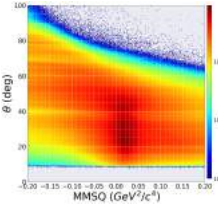

θ BEFORE

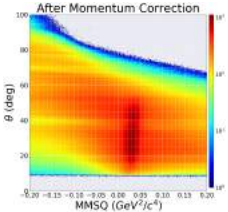

θ AFTER

Energy Loss Correction (ELOSS)

- The ELOSS computes energy loss of the outgoing particles while traveling inside:
  - The butanol target, target cell wall, mixing chamber, holding coils, start counters, and the air gap between DC Region 1

- The ELOSS computes the pathlength inside the materials and computes energy loss via Bethe-Block eq.:

$$-\frac{dE}{dx} = Kz^2 \frac{Z}{A}\frac{1}{\beta}\left[\frac{1}{2}\ln\left(\frac{2m_e c^2\beta^2\gamma^2 T_{max}}{I^2}\right) - \beta^2 - \frac{\delta}{2}\right],$$

- Most significant changes seen in particles with $p \leq 350$ MeV.

- $M^2_{\pi^0}$ peak improved from 0.034 GeV^2 to 0.017 GeV^2 closer to the actual value 0.0182 GeV^2
- The z-vertex dependence of M^2_X distri. inside the butanol target region have been remedied.

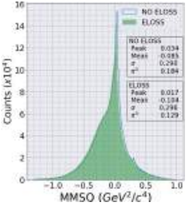

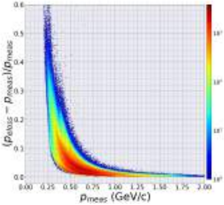

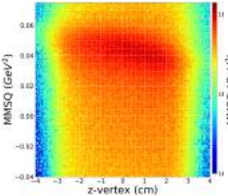

M^2_X BEFORE

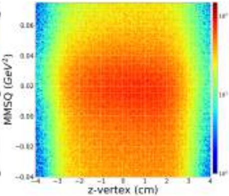

M^2_X AFTER

Momentum Correction

- Momentum correction software for outgoing π^+ in $\gamma p \to \pi^+ n$ [Strauch, 2014]
  -applied to our protons $\to$ no impact on final result.
- ϕ dependence remedied.
- Improved $M^2_{\pi^0}$ peak, but induced θ dependence.
  -deflection different for π^+ and proton
- Difference of measured momentum from the DC (p_{dc}) and calculated momentum ($p(\theta_{lab})$)
  -under assumption that θ is correct.

$$\Delta p = p(\theta_{lab}) - p_{dc}$$

$$\Delta p = \sum_{n=0}^{5} \sum_{m=0}^{2} \sum_{l=0}^{2} a^{n_{sec}}_{n,m,l} \left(\frac{\theta_{lab}}{180^o}\right) \left(\frac{\phi^{sec}_{lab}}{30^o}\right)^m \left(\frac{p_{dc}}{2\ \mathrm{GeV}}\right)^l .$$

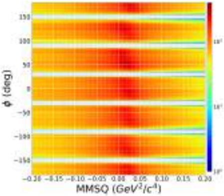

ϕ BEFORE

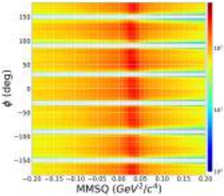

ϕ AFTER

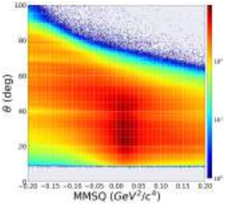

θ BEFORE

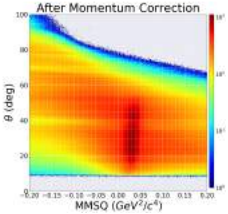

θ AFTER

Inactive CLAS regions

- $\theta_{lab} \leq 7°$,
- $\phi \in [-155°, -145°] \cup [-95°, -85°] \cup [-35°, -25°] \cup [25°, 35°] \cup [85°, 95°] \cup [145°, 155°]$.

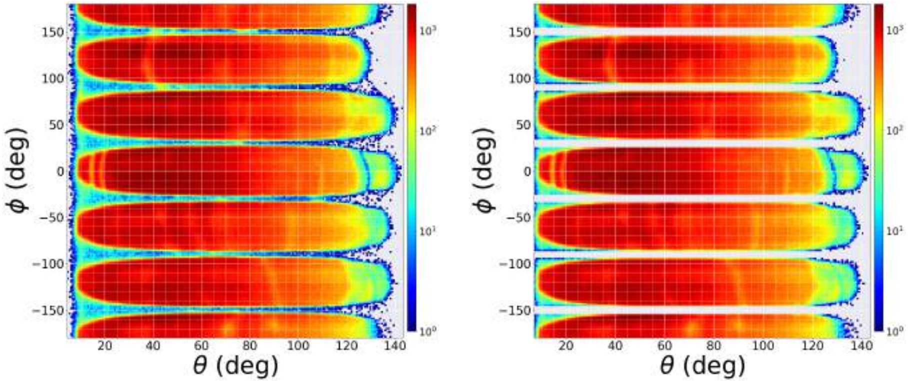

(a) Before (b) After

Low Momentum Selection

- Particles with $p \leq 300$ MeV do not reach the drift chambers
- Particles with low velocity under stronger magnetic field will deflect stronger.
  Too much deflection $\longrightarrow$ Miss TOF panels $8^\circ \leq \theta \leq 142^\circ$
- Holding magnet of 0.5 T in beam axis during the g9a/FROST.
  - $p \leq 350\ MeV/c$ for $\theta_{lab} \geq 35^\circ$,
  - $p \leq 400\ MeV/c$ for $\theta_{lab} \leq 35^\circ$.

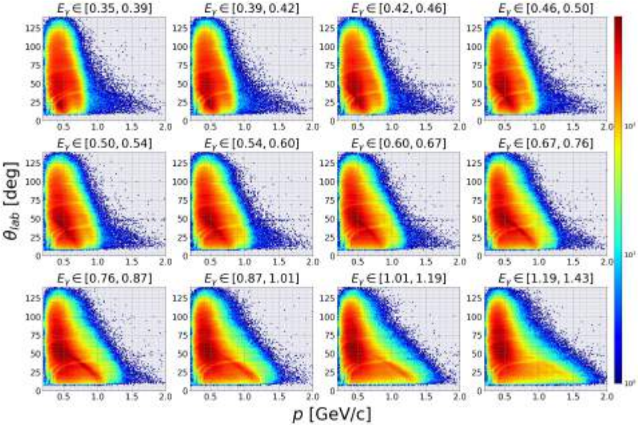

Low Momentum Selection cont.

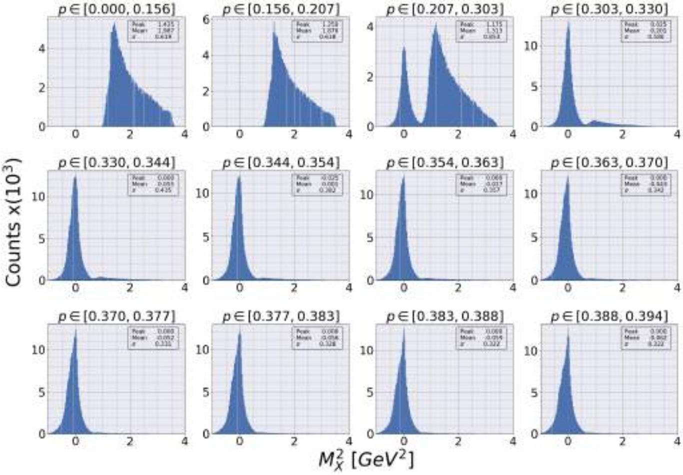

Inefficient Time-of-Flight paddles

Sector	Removed TOF Paddle
1	None
2	38, 44
3	23, 35, 44
4	23, 32, 35, 36, 40, 42
5	23
6	44, 46

(a) Run periods 1, 2, 3, 4 & 5

Sector	Removed TOF Paddle
1	17, 24, 26, 36
2	44, 46
3	23, 35
4	23, 42, 49
5	23, 52, 53
6	44, 46

(b) Run periods 6 and 7

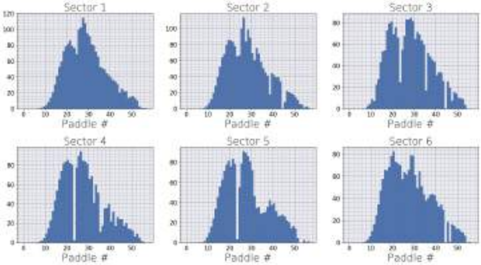

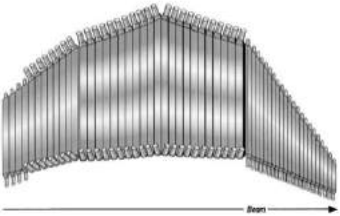

Particle ID: Proton Selection

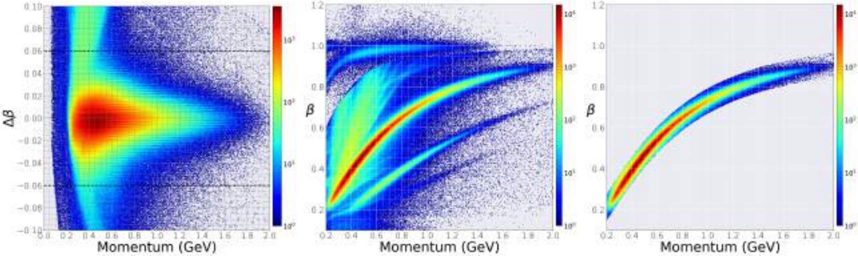

- Measured velocity β_{measured} from TOF and Start counters
- Calculated velocity β_{calc} by assuming outgoing particles as protons and measured p_{dc} from DC.
- $|\Delta\beta| < 0.06$

$$\Delta\beta = \beta_{meas} - \beta_{calc}$$

$$\beta_{meas} = \frac{\text{pathlength between hit positions of SC and TOF}}{\text{flight time between SC and TOF}},$$

$$\beta_{calc} = \frac{p}{E} = \frac{p_{dc}}{\sqrt{p_{dc}^2 + m_p^2}}$$

Photon Identification

- Select photons that caused our $\gamma p \to \pi^0 p$ reaction by time difference of the arriving photons and recoiling protons at z-vertex positions.

$$\Delta t = t_{v,\gamma} - t_{v,p} = \left(t_\gamma + \frac{z}{c}\right) - \left(t_{p,sc} - \frac{l_{sc}}{\beta_{calc} c}\right),$$

$t_{v,\gamma}$	photon arrival time at event vertex,
$t_{v,p}$	reaction time of proton at event vertex
t_γ	photon arrival time at CLAS center
$t_{p,sc}$	arrival time of proton at TOF
l_{sc}	distance from the event to TOF counter.

- Electron beam bunches separated by 2.004 ns intervals
  - Remove photons whose arrival times lie outside of ± 1 ns interval
- About 3% of the total $\gamma p \to \pi^0 p$ events have multiple good photon events $\to$ Removed

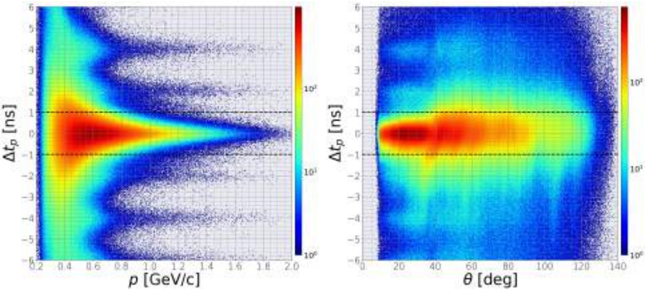

Z-vertex Selection

- Butanol (C_4H_9OH), carbon (C) and polythene (CH_2) targets
- Z event vertex position reconstructed:
  - -Extrapolated particle trajectory's closest distance to the measured center of the beam axis.

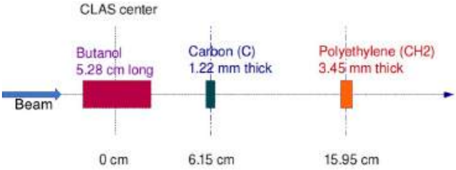

Target	z-vertex min (cm)	z-vertex max (cm)
Butanol	-3	3
Carbon	5	8

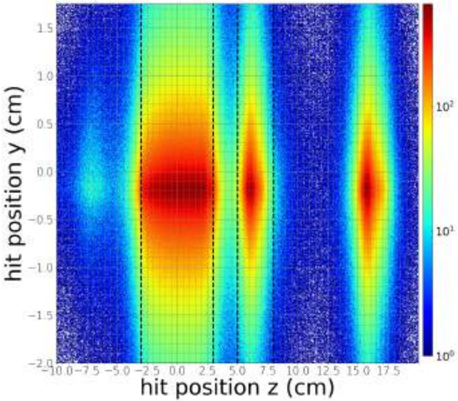

Transverse vertex selection

- 1.5 cm diameter target cup
- Outside events - photons scattering on $^3He - ^4He$ in the dilution refrigerator.
- 3% of total events lie outside of the target cup
- Selection range: $((x - x_{max})^2 + (y - y_{max})^2) < (1\ cm)^2$

  -slighter larger to account for tracking uncertainty

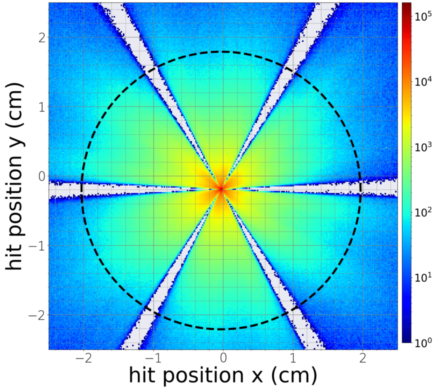

M_X^2 Selection cont. 1

- Maximum scattering angle θ_{p_r} of recoiling protons increases as E_γ increases:

$$\cos(\theta_{p_r}) = \frac{E_\gamma - \left[(E_\gamma + m_{p_1} - E_{p_r})^2 - m^2_{\pi^0}\right]^{1/2}\cos(\theta_{\pi^0})}{|\vec{p}_{p_r}|},$$

- π^0 peaks become more distinct as E_γ increase
  –Above $E_\gamma \geq 1.6$ GeV, more background contribution from non-resonant terms $\rightarrow$ poor statistics overall

- Total angular coverage increases as E_γ increases. See $\cos(\theta_{cm})$ vs p 2dim histogram.

M_X^2 Selection cont. 2

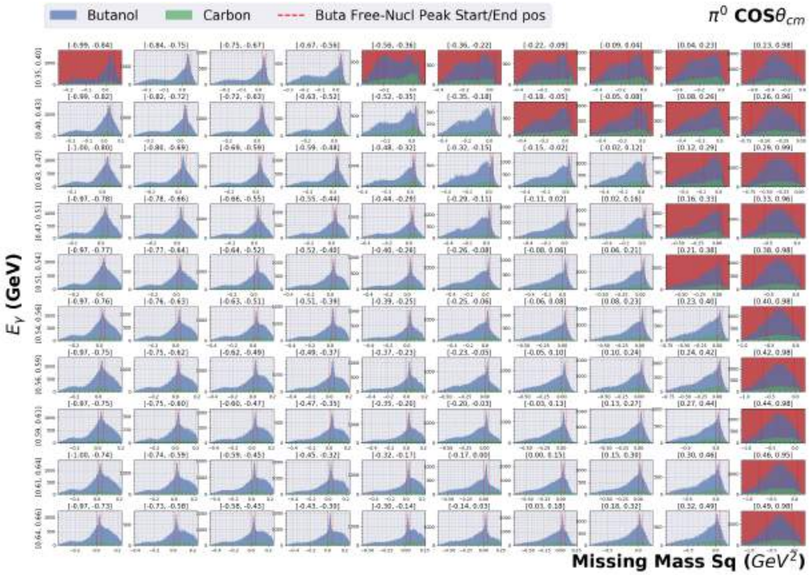

M_X^2 Selection cont. 3

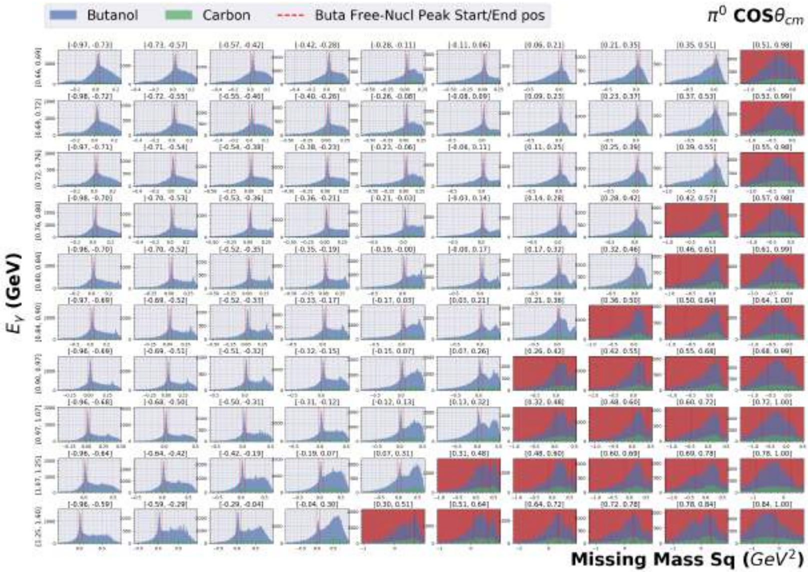

M_X^2 Selection cont. 4

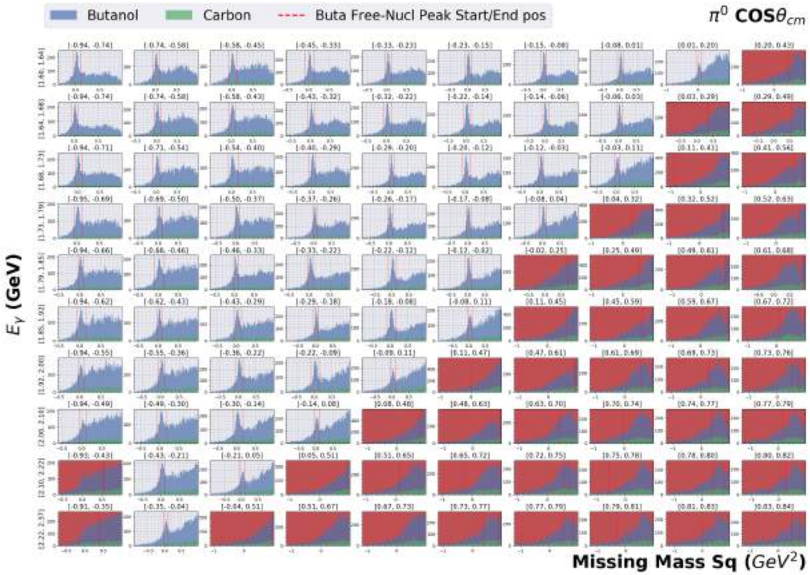

M_X^2 Selection cont. 5

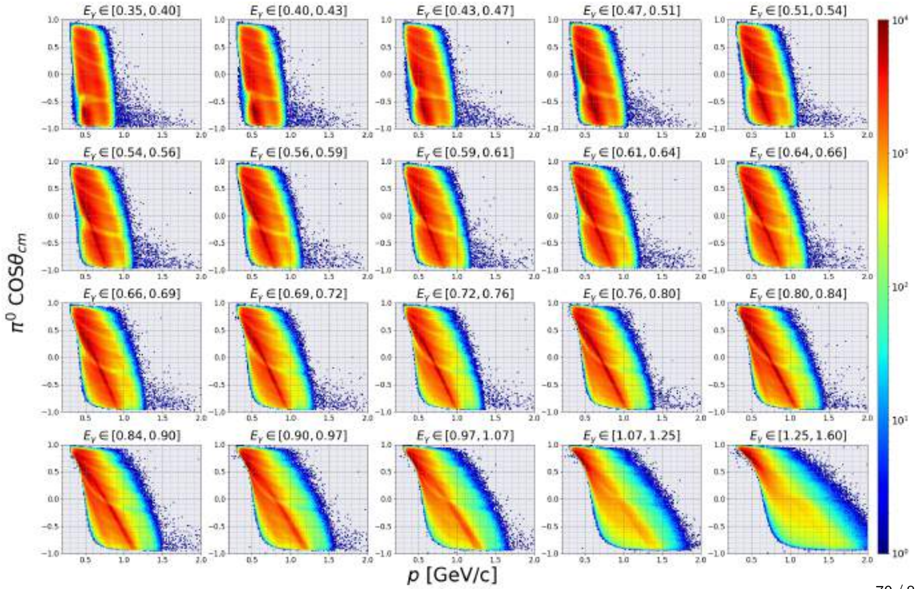

Application of Machine Learning BACK UP

Neural Network Training Flowchart

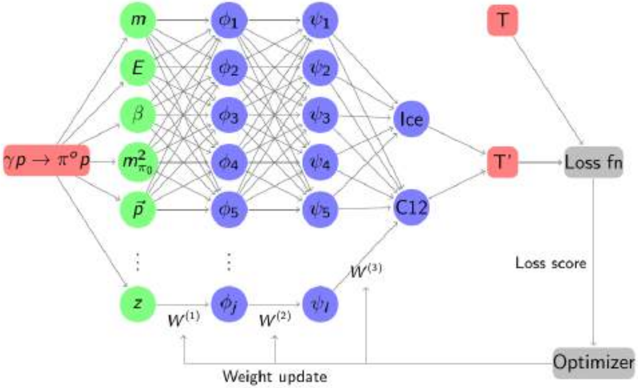

- Fully connected neural layers
- Three hidden layers
- AdamOptimizer
- Loss func.: Sparse categorical cross entropy
  - $H_{y'}(y) = -\sum_i y'_i \log(y_i)$,where y_i is the predicted target and y'_i is the true target

ML Objectives: Target Selection & Ice on Carbon

- Target Classification
  - Events with z-vertex $\in [2, 5]$cm, uncertain whether γ hit Butanol or Carbon

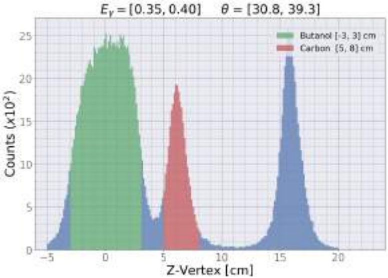

- Ice on Carbon
  - Carbon events (bound-nucleon) expected to have broader $m^2_{\pi_0}$ peak due to Fermi motion.
  - Sharp peak (free-nucleon) observed in the Carbon target region.

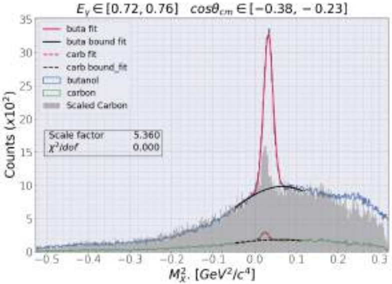

Feature Selection

- Process of selecting parameters used to classify targets.
- No proven rule that guarantees the success of classification.
- Prior knowledge of the parameters
  -constraints on specific parameters (E.g. z)
- Guidelines:
  - High number of parameters & insufficient training data $\rightarrow$ overfit
  - Avoid parameters with significantly low variance $\rightarrow$ less contrib. to classfication
  - Avoid excessive # of highly correlated parameters $\rightarrow$ overfit
    -no white/black on correl. matrix
  - Avoid excessive # of uncorrelated parameters $\rightarrow$ no contrib. to classification

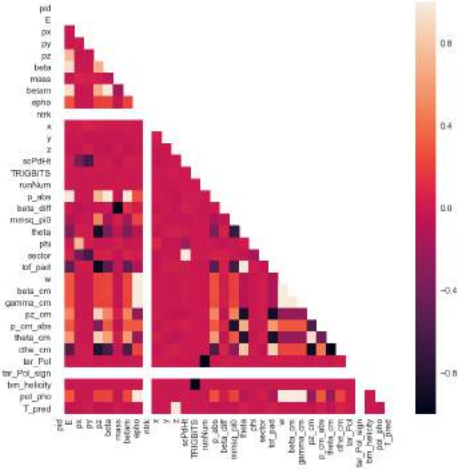

Possible Solutions

- Simulated data as training data.
  - No uncertainty in training data
  - Accuracy of the simulation to real experiments unknown.
  - Detector acceptance, tracking resolution, ELOSS, and momentum correction.
- The g9b/FROST experiment as training data
  - No hydrogen contamination
  - Experimental conditions may differ a lot to g9a/FROST
- Extract ice training data separately in each angle and energy bins
  - Event vertex resolution varies significantly among angular and energy bins
  - Limit training data from $\theta_{lab} \geq 39^\circ$
- Regularization methods to avoid overfitting
  - L1 and L2 method - suppress weights on certain classifying parameters
  - Drop-out method - randomly selects and removes nodes in the hidden layers
  - Early stopping method - Stops training when certain testing error reached.
- Bayesian neural network to quantify uncertainties in training data
  - Pass PDFs in between neural net. layers instead of scalar weights.

Helicity Asymmetry E BACK UP

Steps for Scale factors and Dilution factors

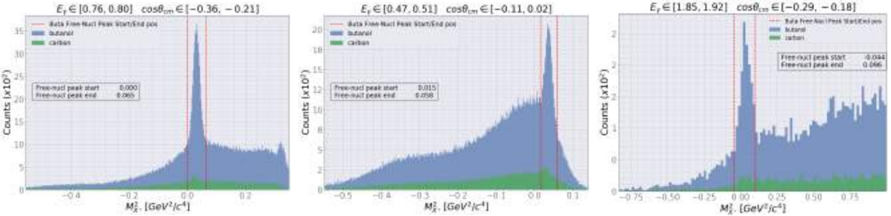

$$S_f = \frac{\#\text{ of background events in buta.}}{\#\text{ of carbon events}} \qquad D_f = \frac{\#\text{ of free nucleon events in buta.}}{\text{Total }\#\text{ of events in buta.}}$$

1. Initial scale factor calculation - direct method
2. First free nucleon peak range extraction
3. Determination of bins to be discarded according to fit results on free nucleon peaks
4. Final Scale Factor calculation
5. Second free nucleon peak range extraction
6. Dilution factor calculation from fitting results.

Initial Scale Factor cont.

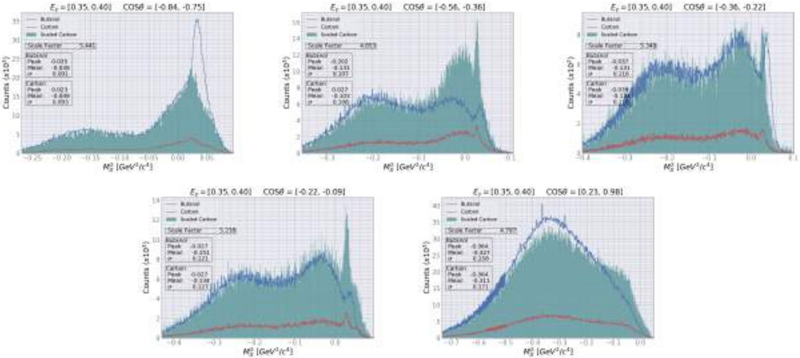

(1) Scaled carbon M_X^2 distribution correctly represents butanol background events.
(2) Angular dependence, causing discrepancies in M_X^2 distributions for butanol and carbon targets.
(3) Background contribution far exceeds free nucleon signals, but still usable if free nucleon ranges are selected out manually
(4) Hydrogen contamination on carbon target where free nucleon peak is visible in carbon distribution
(5) No apparent free nucleon peaks are observed

Discarded Bins cont.

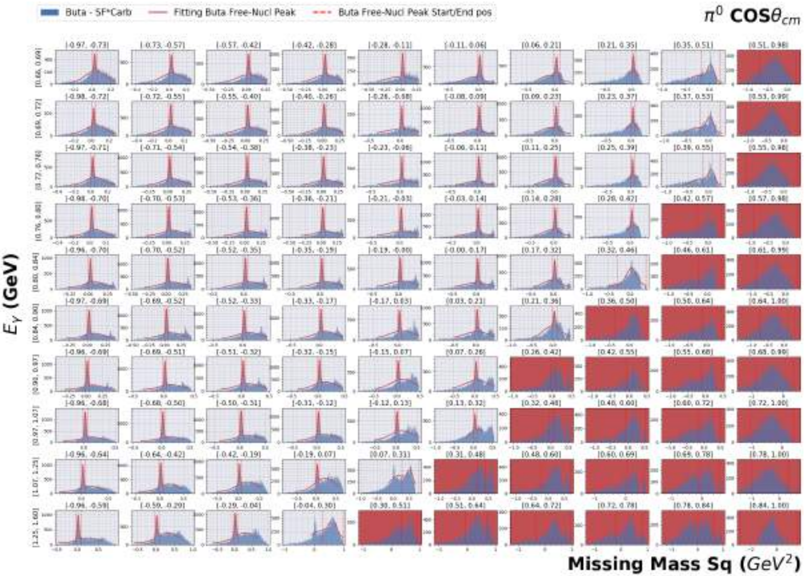

Discarded Bins cont.

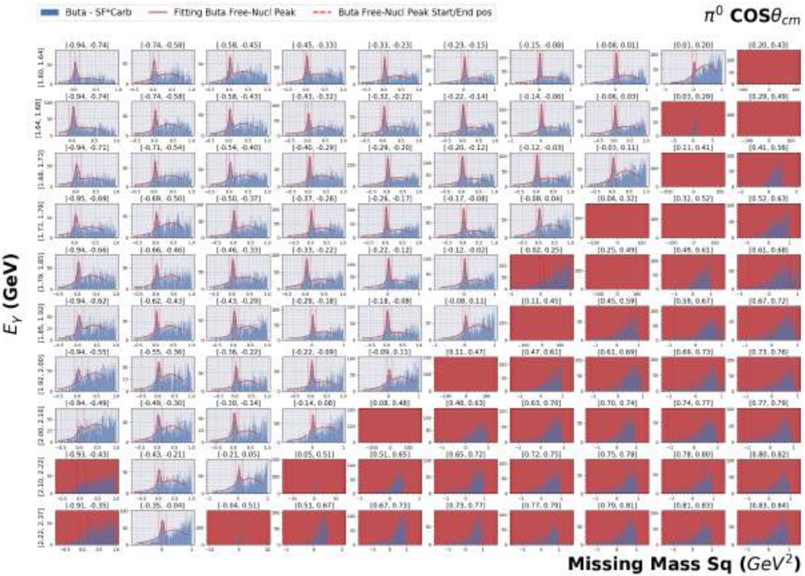

Angular dependence on Scaled carbon

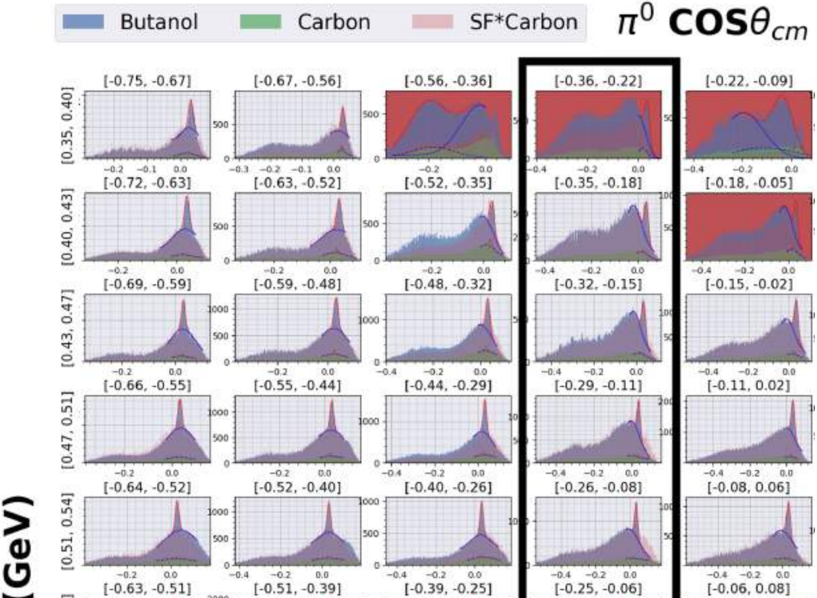

Overview of final butanol free nucleon peak ranges

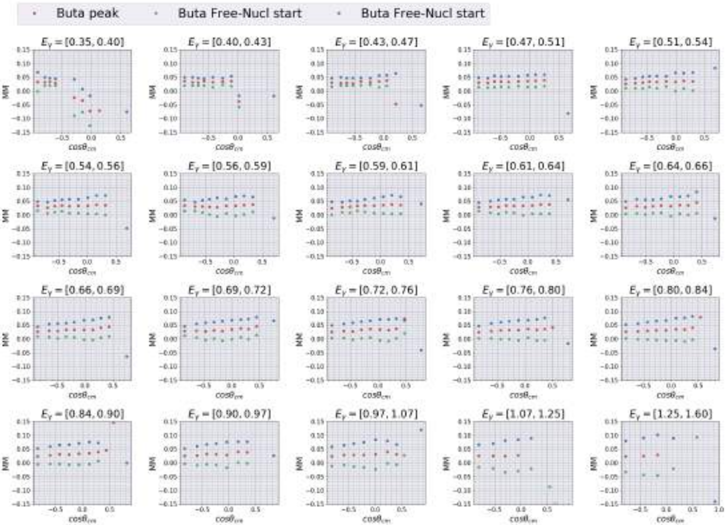

Dilution Factor D_f in $E_\gamma \in [1.6, 2.4]$ GeV

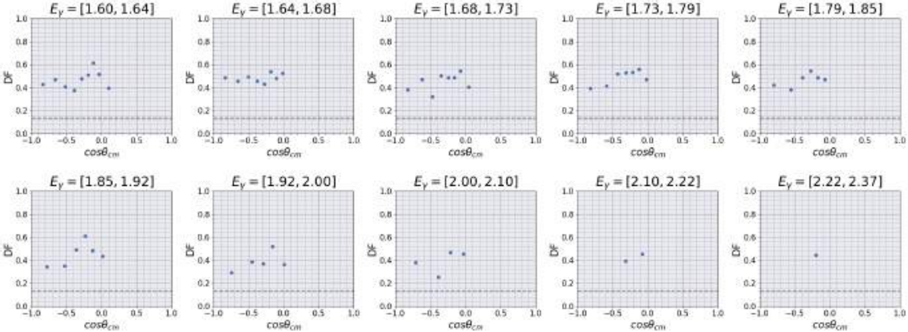

Results BACK UP

Reduced discrepancies between PWA models

- In $E_\gamma = [1.85, 2.4]$ GeV, discrepancies between SAID and BnGa predictions improved.

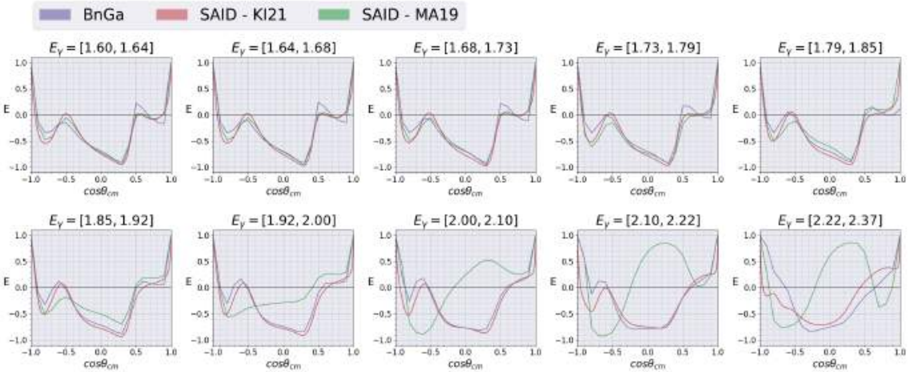

χ^2 per data points in SAID fits

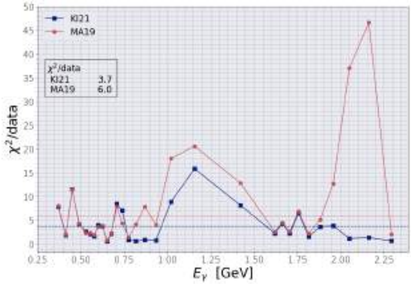

- Normalization constant X for each angular distributions during SAID fitting process.
- χ^2 minimized during the fit:

$$\chi^2 = \sum_i \left[\frac{X\theta_i - \theta_i^{expt}}{\epsilon_i} \right]^2 ,$$

- θ_i^{expt} is individual measurement, θ_i is corresponding SAID prediction, and ϵ_i is the stat. uncertainty for the measurement.
- Average χ^2 per data point improved:
  KI21 ($<\chi^2/data>= 3.7$) and MA19 ($<\chi^2/data>= 6.0$)